ACS APPLIED MATERIALS & INTERFACES

www.acsami.org

Research Article

BODIPY-Based Polymers of Intrinsic Microporosity for the Photocatalytic Detoxification of a Chemical Threat

Ahmet Atilgan, Yassine Beldjoudi, Jierui Yu, Kent O. Kirlikovali, Jacob A. Weber, Jian Liu, Dahee Jung, Pravas Deria, Timur Islamoglu, J. Fraser Stoddart, Omar K. Farha,* and Joseph T. Hupp*

Cite This: *ACS Appl. Mater. Interfaces* 2022, 14, 12596−12605

Read Online

ACCESS | Metrics & More | Article Recommendations | Supporting Information

ABSTRACT: Effective heterogeneous photocatalysts capable of detoxifying chemical threats in practical settings must exhibit outstanding device integrity. We report a copolymerization that yields robust, porous, processible, chromophoric BODIPY (BDP; boron-dipyrromethene)-containing polymers of intrinsic microporosity (BDP-PIMs). Installation of a pentafluorophenyl at the meso position of a BDP produced reactive monomer that when combined with 5,5,6,6-tetrahydroxy-3,3,3,3-tetramethyl-1,1-spirobisindane (TTSBI) and tetrafluoroterephthalonitrile (TFTPN) yields **PIM-1**. Postsynthetic modification of these polymers yields **Br-BDP-PIM-1a** and **-1b**—polymers containing bromine at the 2,6-positions. Remarkably, the brominated polymers display porosity and processability features similar to those of H-BDP-PIMs. Gas adsorption reveals molecular-scale porosity and Brunette−Emmet−Teller surface areas as high as 680 m^2 g^{-1}. Electronic absorption spectra reveal charge-transfer (CT) bands centered at 660 nm, while bands arising from local excitations, LE, of BDP and TFTPN units are at 530 and 430 nm, respectively. Fluorescence spectra of the polymers reveal a Förster resonance energy-transfer (FRET) pathway to BDP units when TFTPN units are excited at 430 nm; weak phosphorescence at room temperature indicates a singlet-to-triplet intersystem crossing. The low-lying triplet state is well positioned energetically to sensitize the conversion of ground-state (triplet) molecular oxygen to electronically excited singlet oxygen. Photosensitization capabilities of these polymers toward singlet-oxygen-driven detoxification of a sulfur-mustard simulant 2-chloroethyl ethyl sulfide (CEES) have been examined. While excitation of CT and LE_{BDP} bands yields weak catalytic activity ($t_{1/2}$ > 15 min), excitation to higher energy states of TFTPN induces significant increases in photoactivity ($t_{1/2} \cong$ 5 min). The increase is attributable to (i) enhanced light collection, (ii) FRET between TFTPN and BDP, (iii) the presence of heavy atoms (bromine) having large spin−orbit coupling energies that can facilitate intersystem crossing from donor−acceptor CT-, FRET-, or LE-generated BDP singlet states to BDP-related triplet states, and (iv) polymer triplet excited-state sensitization of the formation of CEES-reactive, singlet oxygen.

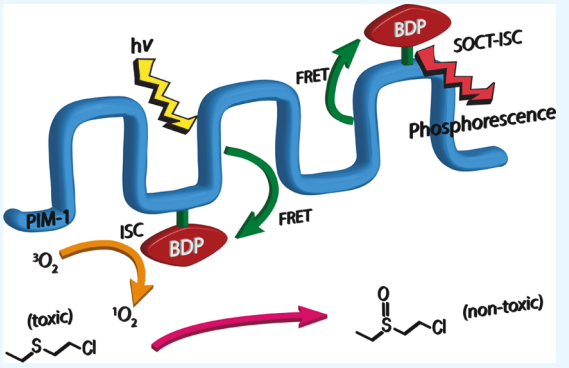

KEYWORDS: *BODIPY, polymers of intrinsic microporosity, sulfur-mustard detoxification, photocatalysis, singlet oxygen, charge and energy transfers*

INTRODUCTION

Since the initial use of chlorine gas as a chemical warfare agent (CWA) in Ypres, Belgium, during World War I (WWI), many CWAs have been developed, produced, stockpiled, and several have been used.[1] A worldwide convention banning the use of chemical weapons has been ratified by all but 3 of the nearly 200 members of the United Nations and has been in force since 1997. Despite the convention, CWAs have since been used by both signatories and nonsignatories, as well as non-nation-state groups, with the targets including both military and civilian populations.[2,3] Consequently, a need exists for protective equipment, including gas masks, suits, gloves, and air filters, that can rapidly detoxify these agents.[4]

Potentially capable of addressing these threats are appropriately functionalized, porous organic polymers (POPs). These materials typically are covalently cross-linked and are characterized, therefore, by extended nonswellable or only marginally swellable, three-dimensional networks. On account of their typically high internal surface areas, good chemical stability, and ready structural and compositional tunability,[5] POPs have been investigated extensively for potential application to problems in, for example, energy storage and conversion,[6,7] chemical catalysis,[5,8−11] gas storage and release,[12,13] and chemical separations.[14−16] In this manner, our research team has also investigated polymer design

Received: November 9, 2021
Accepted: February 22, 2022
Published: March 2, 2022

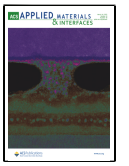

Scheme 1. Synthesis of BDP-Based PIM Derivatives at Different Monomer Ratios[a]

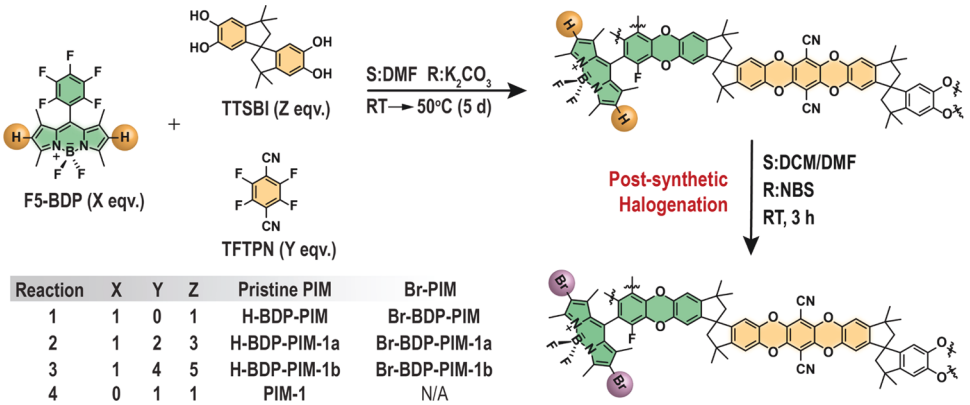

Reaction	X	Y	Z	Pristine PIM	Br-PIM
1	1	0	1	H-BDP-PIM	Br-BDP-PIM
2	1	2	3	H-BDP-PIM-1a	Br-BDP-PIM-1a
3	1	4	5	H-BDP-PIM-1b	Br-BDP-PIM-1b
4	0	1	1	PIM-1	N/A

[a]The inset table shows the monomer ratios in polymerization reactions and the names of the resulting polymers for each reaction entry.

strategies to magnify the low photocatalytic activity of BODIPY-based conjugated POPs.[17] The integration of cross-linked POPs in practical devices, however, remains elusive as, in most cases, poor solubility in both organic and aqueous solvents limits their processability.[18−20] Over the last decade,[21] attention has been devoted to polymers of intrinsic microporosity (PIMs) as a way to bypass these limitations as PIMs are typically soluble in several organic solvents and, as a result, can be processed into membranes, porous films, and porous coatings. In contrast to POPs that achieve porosity via suitable chemical cross-linking, PIMs derive porosity from molecular-scale interstitial spaces that arise from intentionally inefficient packing of contorted polymer chains.[22,23] Although PIMs have been implemented in several applications, a few reports have examined their performance for photochemical transformations.[24,25]

Fluorescent boron-dipyrromethene (BODIPY or BDP) dyes have been extensively studied in a variety of photochemical transformations on account of their excellent chemical tunability, stability in a wide range of conditions, and high solubility in organic solvents.[26−28] For example, researchers have leveraged the optical and chemical stability, high molecular absorption coefficients, efficient singlet oxygen ($^1O_2$) quantum yields, and straightforward optical tunability that is inherent to BDPs to explore applications in photodynamic therapy[26] and photocatalysis.[29,30] For applications that entail photosensitization of $^1O_2$ formation, conversion of the BDP core into an efficient photosensitizer requires boosting its singlet (S) to triplet (T) intersystem crossing (ISC) yield—for example, by incorporating into the BDP core heavy atoms, such as Br and I, which feature strong spin−orbit coupling (SOC).[31] Recently, photoinduced electron transfer (PeT) in electron donor−acceptor BDP-based dyads resulted in efficient ISC due to the SOC-CT of the charge-separated state.[31−34] More recently, a combination of the spin−orbit charge-transfer intersystem crossing (SOCT-ISC) and SOC associated with heavy atoms in the TBP⊂ExBox^{4+} supramolecular host−guest system was shown to enhance the singlet-to-triplet (S-T) spin transformation to enable photocatalysis of CEES (2-chloroethyl ethyl sulfide) upon light irradiation.[4] Other investigations have reported the design of chromophoric polymers with efficient Forster resonance energy transfer (FRET) between chemically distinct donor and acceptor units. Intimately combining these units can be functionally beneficial by (i) harvesting more light from a broad spectral range and (ii) increasing the desired performance of the acceptor unit, such as enhanced brightness for bioimaging[35] or triplet excited-state generation for photodynamic therapy applications.[36]

Herein, we describe the design and synthesis of BDP-containing PIMs (Scheme 1) that combine strong light absorption by the PIM backbone with complementary absorption and efficient photosensitization of singlet oxygen formation by pendant BDP units. In addition, the PIM backbone imparts porosity and processability, affording robust yet permeable materials capable of detoxifying the sulfur-mustard simulant CEES under visible light irradiation. Specifically, pentafluorophenyl-substituted BODPIY was copolymerized in varying proportions with 5,5,6,6-tetrahydroxy-3,3,3,3-tetramethyl-1,1-spirobisindane (TTSBI or spirobisindane) and tetrafluoroterephthalonitrile (TFTPN) to form **H-BDP-PIM-1a** and **H-BDP-PIM-1b** in high yield. Subsequent treatment with *N*-bromosuccinimide (NBS) installs Br atoms at the 2,6- positions of the BDP moieties, which boosts photocatalytic performance due to spin−orbit-coupling-enhanced intersystem crossing. We investigated the optical properties of the materials via electronic absorption (UV−vis) and emission spectroscopies, including time-resolved fluorescence spectroscopy. The electronic characteristics of the polymers were deciphered, in part, by performing density functional theory (DFT) calculations. Finally, we explored the efficacy of the polymers as photocatalysts for oxidation (oxygenation) of CEES, both in bulk solution, and in the case of **Br-BDP-PIM-1b**, as a thin-film heterogeneous photocatalyst, ultimately confirming that the compounds comprise a promising new class of photocatalysts capable of detoxifying sulfur-based chemical threats.

EXPERIMENTAL SECTION

The details about the synthesis protocols and experimental methods are described in the Supporting Information. Each polymer's photocatalytic performance in solution toward CEES oxidation was tested as follows: 2.5 mg (0.8 wt %) of polymer was weighed directly into a Biotage high-precision microwave vial (2−5 mL) equipped with a magnetic stir bar, and the vial was successively sealed with a crimper. CD_3OD (1 mL) was injected into the vial through its rubber seal. The mixture was bubbled with O_2 gas for 20 min using inlet and outlet needles. The sealed mixture under ca. 1 bar oxygen was shortly sonicated until the catalyst mixture had a good dispersion. Finally, CEES (23 μL, 0.2 mmol) was added via a 50 μL microsyringe through the rubber seal. The microwave vial was placed between two LEDs

https://doi.org/10.1021/acsami.1c21750
ACS Appl. Mater. Interfaces 2022, 14, 12596−12605

bearing royal blue, green, or red solderless LEDs, fixed on a U-shaped aluminum plate, and photoirradiated for particular time intervals. Aliquots were taken at different time intervals during the reaction and moved in 1.5 dram vials. Then, 0.5 mL of CD_3OD aliquots was added and transferred to an NMR tube for ^1H and ^{13}C NMR analysis.

The photocatalytic oxidation of CEES on the surface was conducted as described: the polymer-coated microscope slide was placed facing upward in a flat-bottom vial. Neat CEES (0.5 μL) was initially added to 100 μL of oxygenated CD_3OD in a separate container using a microsyringe, and then the resulting solution was carefully spread over the polymer-coated microscope slide sitting in the vial using a micropipette. The vial was lightly capped and positioned between two LEDs fixed on the U-shaped aluminum plate. Upon completion of photoexcitation, 0.5 mL of fresh CD_3OD was added to this vial to collect the reaction components, and this mixture was transferred into an NMR tube for ^1H and ^{13}C NMR analysis. This process was repeated for each data point.

RESULTS AND DISCUSSION

Synthesis and Structural Characterization. The BDP-based PIMs (H-BDP-PIMs) were polymerized according to the procedure reported by Budd and co-workers to synthesize **PIM-1**.[37] Specifically, dimethylformamide (DMF) solutions containing the pentafluorophenyl-substituted BDP, F5-BDP, and the **PIM-1** monomers, TTSBI and TFTPN, were stirred with potassium carbonate at room temperature for a day and then the temperature was increased to 50−55 °C over the course of several days (Scheme 1). Relatively low reaction temperatures are essential for this system as the $-BF_2$ moiety of the BDP is susceptible to substitution in the presence of nucleophiles at elevated temperatures.[38] Substitution of BDP with spirobisindane can yield a cross-linked polymer with low solubility.[39] Increases in the proportion of TFTPN in the reaction mixture affords more soluble polymers. The Supporting Information shows more details regarding the solubility properties of all polymers (Table S1).

Once isolated, the structures of the polymers were corroborated through analysis of ^1H, ^{11}B, and ^{19}F NMR spectra (see the Supporting Information for more details). Specifically, broad singlets arising at approximately 6.02 ppm in the ^1H NMR spectra of BDP-based polymers correspond to the hydrogen atoms connected to the BDP core at the 2,6-positions. Additionally, BDP methyl protons appear at ∼2.54 ppm, while broad peaks attributed to the spiroindane comonomer are observed at 6.8 and 6.4 ppm, which is consistent with the chemical shifts for the aromatic peaks in the ^1H NMR spectrum of **PIM-1** (Figure S4). Similar ^1H NMR spectra are observed for all nonhalogenated polymers incorporating BDP units as they only differ in the ratios of monomers used during the polymerizations (ratios of F5-BDP/TFTPN/TTSBI = 1:0:1 for **H-BDP-PIM**, 1:2:3 for **H-BDP-PIM-1a**, and 1:4:5 for **H-BDP-PIM-1b**). The spirobisindane moiety/BDP ratios in pristine PIMs can be inferred by integrating the peaks at ∼6.42 and ∼6.02 ppm in the ^1H NMR spectrum, resulting in ratios of 1.1, 5.4, and 13 for **H-BDP-PIM**, **H-BDP-PIM-1a**, and **H-BDP-PIM-1b**, respectively. In parallel to the monomer ratio obtained via NMR, the average molecular weights of **H-BDP-PIM**, **H-BDP-PIM-1a**, and **H-BDP-PIM-1b** calculated by gel permeation chromatography (GPC) are found to be 1.7k, 3.0k, and 4.4k Da, respectively (Figure S24). This implies that the increased F5-BDP ratio in the polymerization reaction tends to terminate polymerization. The ^{11}B NMR spectrum of **H-BDP-PIM-1b** reveals only a triplet at 0.7 ppm that is characteristic of the $-BF_2$ group within the BDP core (Figure S11). In contrast, the ^{11}B NMR spectrum of **H-BDP-PIM-1a** consists of a minor singlet at 7.2 ppm, in addition to the major triplet at 0.70 ppm (Figure S7). This chemical shift is consistent with the presence of a catechol-substituted BDP,[38] as peaks corresponding to these products have been observed as singlets approximately at 7.3 ppm in ^{11}B NMR spectra depending on the substituent on the catechol.[40]

Analysis of the ^{19}F NMR spectra of the polymers reveals that the ratio of aromatic fluorine to boron decreases with increasing stoichiometric ratio of TFTPN in the polymerization reactions, suggesting that F5-BDP reacts at the terminal positions of the polymer chains when copolymerizing with TFTPN (see the Supporting Information for related NMR spectra). These reactivity trends are consistent with those reported in the literature,[41,42] as strongly electron withdrawing and relatively less sterically hindered cyano groups on TFTPN activate this substrate and, as a result, the kinetics of the nucleophilic aromatic substitution reactions on TFTPN are favored relative to those of BDP-substitution on the pentafluorophenyl group.

Bromination of pristine PIMs at the 2,6-positions of the BDP units was achieved postsynthetically following a previously reported procedure,[17] in which *N*-bromosuccinimide (NBS) is used as the bromine source in a mixture of CH_2Cl_2/DMF at room temperature (see the Supporting Information for full experimental details). ^1H NMR spectra for **Br-BDP-PIM**, **Br-BDP-PIM-1a**, and **-1b** indicate that complete conversion to the brominated products as the peak at about 6 ppm, which corresponds to the H atoms at 2,6-positions in the BDP core, is absent for all three polymers following NBS treatment (see Figures S12, S15, and S18). Furthermore, bromination results in not a significant difference in the ^{19}F and ^{11}B NMR spectra of the polymers, suggesting an absence of undesired side reactions (see the Supporting Information).

Next, we employed X-ray photoelectron spectroscopy (XPS) to determine the amounts of C, N, O, F, and Br present in each polymer (Table 1). First, we found that after bromination of the pristine polymers, the bromine content in each polymer increases in the order of **Br-BDP-PIM** > **Br-BDP-PIM-1a** > **Br-BDP-PIM-1b**, which mirrors the relative number of BDP chromophores present in each pristine polymer as determined by the corresponding ^1H NMR spectrum. The N/F atomic percent ratios for **Br-BDP-PIM**, **Br-BDP-PIM-1a**, **Br-BDP-PIM-1b** are 0.5, 1.3, and 1.9, respectively. The increase in the N/F ratio for the series is associated with the nitrogen atoms on the TFTPN monomer as the reaction conditions for **H-BDP-PIM-1b** included twice the number of equivalents of

Table 1. XPS Atomic Percent Distribution of Selected Elements in Polymer Samples

samples	C	N	O	F	Br	Br/F	N/F
PIM-1	82.5	4.2	13.2	0.0	0.0	n/a	n/a
H-BDP-PIM	75.0	4.3	11.7	9.0	0.0	0.0	0.5
H-BDP-PIM-1a	79.6	4.7	12.1	3.6	0.0	0.0	1.3
H-BDP-PIM-1b	81.1	4.7	11.3	2.9	0.0	0.0	1.6
H-BDP-PIM-1a-65	80.9	4.4	12.9	1.8	0.0	0.0	2.4
Br-BDP-PIM	72.9	4.1	11.1	8.8	3.0	0.3	0.5
Br-BDP-PIM-1a	79.0	4.2	12.6	3.2	0.9	0.3	1.3
Br-BDP-PIM-1b	80.6	4.4	11.8	2.4	0.8	0.3	1.9

https://doi.org/10.1021/acsami.1c21750
ACS Appl. Mater. Interfaces 2022, 14, 12596−12605

TFTPN relative to those used for **H-BDP-PIM-1a**. Spirobisindane substitution on $-BF_2$ positions is also partly responsible for the differences in these ratios. In line with the ^1H NMR data, when the **F5-BDP** ratio increases in the polymerization reaction, the S_N2 reaction on the boron atom of BDP becomes more apparent, in addition to the desired nucleophilic aromatic substitution at a given temperature. Moreover, when the polymerization reaction is performed at 65 °C, the resultant polymer **H-BDP-PIM-1a-65C** shows almost double the N/F ratio (2.4) of **H-BDP-PIM-1a** (1.3), which is polymerized at 50−55 °C. Thus, increasing polymerization temperatures results in more of the undesired S_N2 substitutions on the boron atoms of BDP. Finally, the Br/F ratios of ∼0.3 for all three brominated polymers are consistent with bromination occurring only on BDP units.

According to thermogravimetric analysis (TGA) data (Figure S23), **PIM-1** shows the highest thermal stability, with onset decomposition being observed at ca. 490 °C and above, as also seen in the literature.[43] In contrast, the temperature inflection for decomposition of **H-BDP-PIM** starts at slightly below ∼200 °C. The polymers differ in the inclusion of F5-BDP monomers in the presence of TFTPN, which leads to a decrease in the thermal stability of the resulting polymers. Furthermore, the polymers constructed from both TFTPN and F5-BDP monomers show decomposition footprints of both **PIM-1** and **H-BDP-PIM**. The overall thermal stabilities of these polymers improve with increasing amounts of dicyanobenzene groups (from the TFTPN-based moiety) in the polymer backbone (**H-BDP-PIM-1b** > **H-BDP-PIM-1a**). Analysis of the TGA curve for **H-BDP-PIM-1a-65C** reveals a slightly lower degradation temperature in the BDP and polymer backbone region (ca. 475 °C) compared to that of **H-BDP-PIM-1a** and is associated with the cross-linked structure of the former material. The halogenated polymers degrade faster than nonhalogenated versions due to the presence of bromine atoms in the structure. Parallel to their pristine polymers, the TGA curves for **Br-BDP-PIM-1a** and **Br-BDP-PIM-1b** feature similar onsets for decomposition but different decomposition ratios, and their thermal stabilities outperform that of the TFTPN-free **Br-BDP-PIM**.

Gas Adsorption. Following activation of each sample at 80 °C for 18 h, N_2 adsorption−desorption isotherms were collected at 77 K for **H/Br-BDP-PIM** and **H/Br-BDP-PIM-1b**, and CO_2 adsorption−desorption isotherms were collected at 195 K for **H/Br-BDP-PIM-1a** (Figure 1). All samples exhibit a Type I isotherm hysteresis, as defined by the International Union of Pure and Applied Chemistry (IUPAC).[44] The steep uptake observed at low pressures is indicative of a microporous structure. Larger pores are also present in these polymeric structures. The Brunauer−Emmett−Teller (BET) surface areas of **H-BDP-PIM-1b** and Br-BDP-PIM-1b are 620 and 680 $m^2\ g^{-1}$, respectively, and the pore size distributions calculated for **H/Br-BDP-PIM-1b** using nonlocal density functional theory (NLDFT) show that the major pore volume contributions result from pores smaller than 10 Å, although **H-BDP-PIM-1b** also exhibits multiple pores larger than 20 Å as well (Figure S22). Although bromination of nonhalogenated polymers increases the average molecular weight of the polymers, gravimetric nitrogen uptake increases upon bromination for both Br-BDP-PIM-1b and Br-BDP-PIM relative to that of the nonbrominated analogues. This counterintuitive behavior is attributed to the relatively lower packing efficiency that results from the introduction of

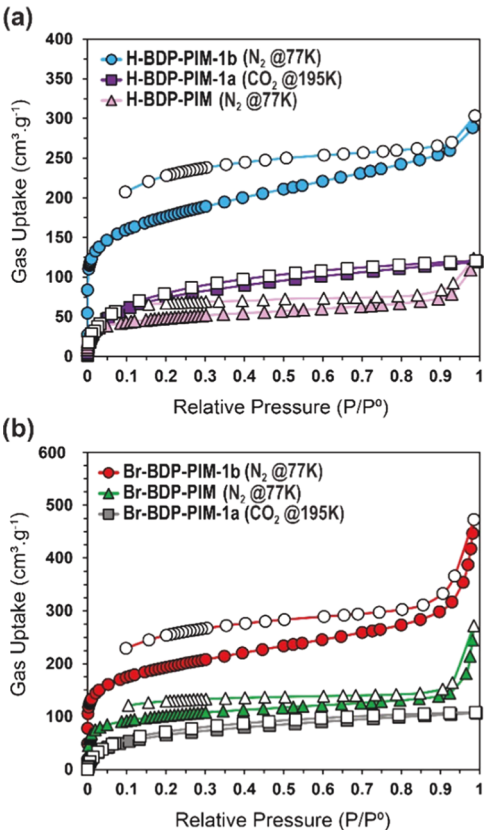

Figure 1. Nitrogen sorption isotherms of polymers at 77 K and given relative pressures. Filled and hollow markers represent adsorption and desorption, respectively. (a) BET surface areas for **H-BDP-PIM-1b** and **H-BDP-PIM** are 620 and 170 $m^2\ g^{-1}$, respectively. (b) BET surface areas for **Br-BDP-PIM-1b** and **Br-BDP-PIM** are 680 and 360 $m^2\ g^{-1}$, respectively. Carbon dioxide sorption isotherms of **H** and **Br-BDP-PIM-1a** at 195 K. BET surface areas for **H** and **Br-BDP-PIM-1a** are 370 and 325 $m^2\ g^{-1}$, respectively.

the much more sterically encumbered bromides onto the BDP units. For example, H- and Br-BDP-PIM, which contain the largest BDP/spirobisindane ratio among all polymers, show the largest difference between the BET surface areas for the pristine and brominated polymers among this set as the surface area almost doubles from 170 to 360 $m^2\ g^{-1}$ upon bromination.

In contrast, the polymers with the relatively lowest BDP content, **H**, and **Br-BDP-PIM-1b**, demonstrate the smallest increase in the BET surface area upon bromination (620 and 680 $m^2\ g^{-1}$, respectively). Finally, **H** and **Br-BDP-PIM-1a** show a Type I isotherm with increasing CO_2 adsorption under low pressure at 195 K, and the BET surface areas of the pristine and daughter polymers are 370 and 325 $m^2\ g^{-1}$, respectively. Overall, these gas adsorption studies indicate that the ratio of BDP/spirobisindane is inversely proportional to the surface area of the polymers (i.e., relatively higher BDP content results in lower BET surface areas) as a result of greater polymer flexibility at higher BDP/spirobisindane ratios.

Photophysical Studies. The UV−vis absorption spectra for **F5-BDP** and **PIM-1** reveal absorption maxima at 433 and 516 nm, respectively (Figure S25). The similar absorption maxima observed in the UV−vis spectra for **H-BDP-PIM**, **H-BDP-PIM-1a**, and **H-BDP-PIM-1b** suggest that both the BDP- and spirobisindane-based chromophores remain largely unaltered by polymerization (Figures 2a,d and S26).

https://doi.org/10.1021/acsami.1c21750
ACS Appl. Mater. Interfaces 2022, 14, 12596−12605

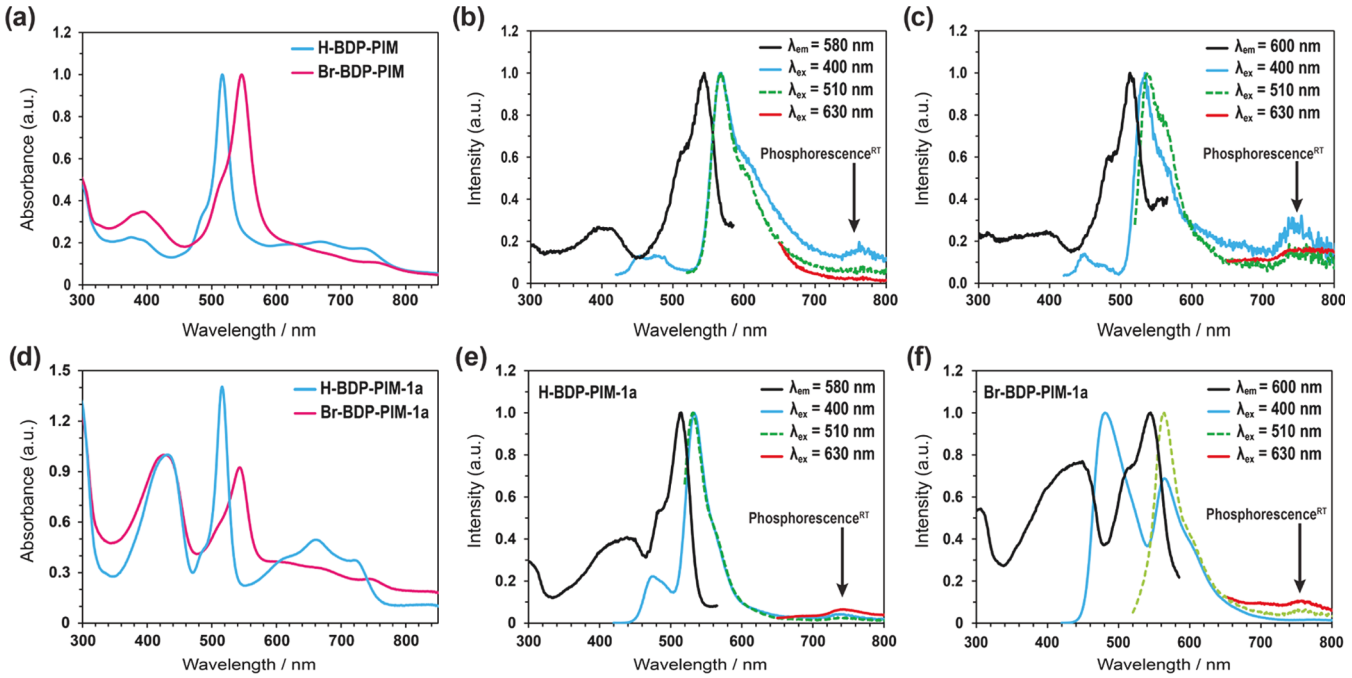

Figure 2. (a, d) Absorbance spectra of the polymers. (b, e) Emission and excitation spectra of **H-BDP-PIM** and **H-BDP-PIM-1a**. (c, f) Emission and excitation spectra of **Br-BDP-PIM** and **Br-BDP-PIM-1a**. UV−vis spectra were recorded in THF under ambient conditions. All emission spectra were recorded in degassed THF at room temperature in an oxygen-free environment. Phosphorescence was observed for BDP-PIMs at different intensities.

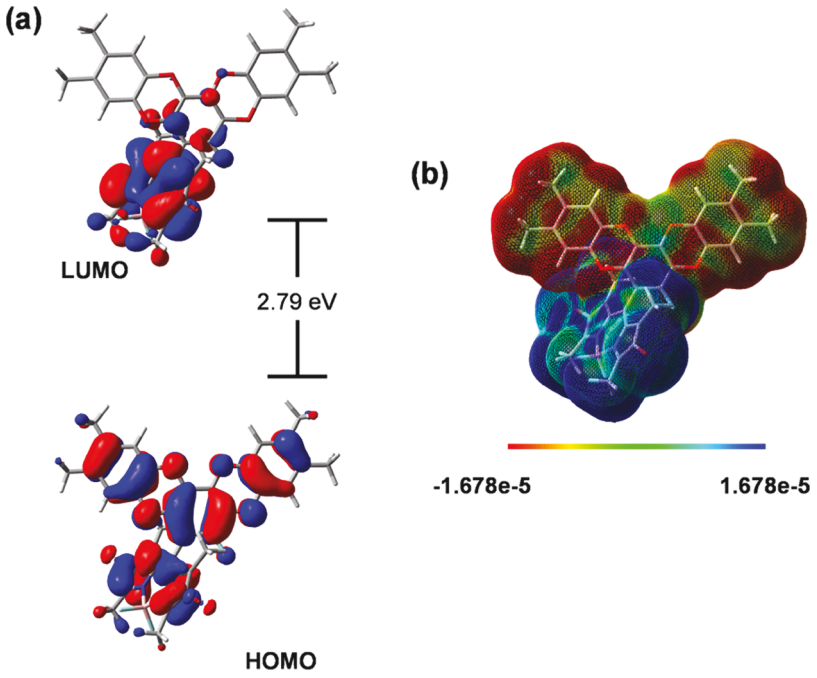

Figure 3. (a) DFT-calculated highest occupied molecular orbital−lowest unoccupied molecular orbital (HOMO−LUMO) energy levels and electron distribution of a chromophore obtained by fusing BDP and spirobisindane. (b) Electrostatic potential difference map of the fused BDP-spirobisindane chromophore in the excited state.

Incorporation of Br atoms at the 2,6-positions of the BDP cores of the polymers engenders a red shift (from 516 to 546 nm) in the peak corresponding to the BDP unit—behavior that has been observed in other BDP-containing polymers.[17] It is noteworthy that all of the BDP-PIMs display broad absorption bands in the red region of the spectrum. The bands are associated with charge transfer (CT)[45] from the electron-rich spirobisindane moiety to the electron-poor BDP moiety (vide infra) and thus serve to extend the spectral coverage to a longer wavelength than attainable with the isolated component monomers.

Subsequently, we evaluated ambient temperature photoluminescence. The **F5-BDP** monomer and **PIM-1** polymer exhibit strong emission (fluorescence), with bands centered at

https://doi.org/10.1021/acsami.1c21750
ACS Appl. Mater. Interfaces 2022, 14, 12596−12605

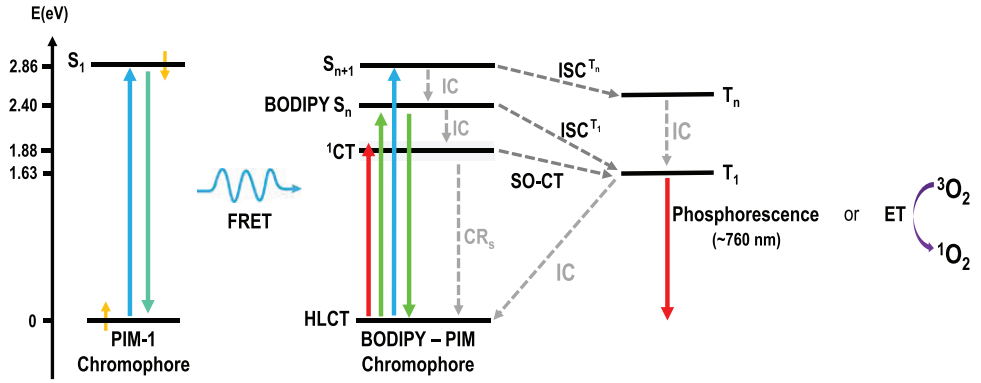

Figure 4. Schematic energy diagram showing the possible pathways of relaxation when brominated BDP-PIM-based polymers are excited under green, blue, and red light. The relaxation path to ^{1}CT from excited BDP S_n level through internal conversion (IC) competes with the ISC path at green-light excitation. FRET populates excited states of the BDP moiety under blue-light photoirradiation of the dicyanobenzene chromophore as observed in **H/Br-BDP-PIM-1a** and **-1b** polymers.

480 nm (Φ_F = 67%, τ_1 = 10.4 ns) and 530 nm, respectively (Figure S25; Tables S2 and S3). Steady-state spectroscopic studies reveal that upon excitation at 400 nm, **H-BDP-PIM**, **H-BDP-PIM-1a**, and **H-BDP-PIM-1b** each display three emission bands, with the bands centered at about 477, 531, and 750 nm (Figures 3b,e and S27). Fluorescence quantum yields (Φ_F) of **H-BDP-PIM**, **H-BDP-PIM-1a**, and **H-BDP-PIM-1b** are 0.14, 5.5, and 7%, respectively; the increases in Φ_F are correlated with increases in the number of TFTPN-based chromophores present in polymer backbones and are indicative of FRET behavior that populates singlet excited states of the BDP moieties. While the emission bands at 477 and 530 nm are associated with fluorescence relaxation from the LE of TFTPN (LE_{TFTPN}) and BDP (LE_{BDP}) units, respectively, the relatively weaker emission band at 750 nm arises from phosphorescence decay from the lowest triplet (T_1) state.

Phosphorescence at room temperature is rare in non-halogenated BDP chromophores, and the increased rigidity that results from the incorporation of BDP units into the polymer backbone of this system likely enables efficient phosphorescence to occur.[46] Furthermore, the S_1 state, which is associated with the CT (^{1}CT), and the T_1 state are close in energy, and an efficient S-T intersystem occurs even in the absence of heavy Br atoms. The relative contribution to the emissive population by energy transfer (energy transfer %) in the polymers is calculated as 81% when **H-BDP-PIM-1a** and **-1b** are excited at 400 nm.

Comprehensive emission data for these polymers, including fluorescence and phosphorescence quantum yields and the corresponding data related to their excited-state lifetimes, are presented in Tables S2 and S3. In all cases, bromination of these polymers leads to a bathochromic shift for the BDP-derived fluorescence (Figures 2b,c, S25, and S26). **Br-BDP-PIM-1a** and **-1b** are characterized by fluorescence quantum yields of 1.8% (τ = 0.9 ns [82%], 3.9 ns [18%]) and 5.2% (τ = 1.7 ns [68%], 7.4 ns [32%]), respectively. The yields are slightly less than those found for their bromine-free congeners, consistent with a role for heavy Br atoms in enhancing singlet decay via intersystem crossing.

DFT Calculations. DFT calculations were performed on the molecular structures of representative chromophore units of each polymer. The results qualitatively reproduce the experimental variations in HOMO−LUMO energy gaps (ΔE; Figure 3). The structures of the BDP-infused chromophores that reside on the polymer backbone and **PIM-1** repeating units were geometrically optimized at the APFD/6-31G(d) level to explicitly include dispersion interactions.[47]

Following geometric optimizations, we studied electronic states using the B3LYP/6-31G(d) level of theory. These calculations show that the HOMO−LUMO band gap is 3.31 eV, and that upon excitation, electrons migrate from the longitudinal axis of the ring system onto the central, cyanophenyl group of **PIM-1** (Figure S34). The electrostatic potential difference map indicates that spirobisindane is electron-rich, while BDP is electron-poor (Figure S33), consistent with the experimental observation of the CT-based absorption from ~580 to 750 nm. DFT calculations on the spirobisindane-substituted BDP component show a HOMO−LUMO energy level gap of 2.79 eV (Figures 3a and S35). The HOMO and the LUMO orbitals are localized on the BDP and spirobisindane moieties, facilitating the charge transfer between them.

Photocatalysis. The photocatalytic performance of each of the polymers toward the oxidation of the moderately toxic sulfur-mustard simulant 2-chloroethyl ethyl sulfide (CEES) to the nontoxic sulfoxide 2-chloroethyl ethyl sulfoxide (CEESO) was monitored under similar experimental conditions to facilitate qualitative comparisons of different polymers. Figure 4 summarizes the proposed mechanism of photosensitization for BDP-PIMs: following light absorption, energy transfer from the polymer backbone (donor) to the BDP (acceptor) moiety results in the production of singlet oxygen ($^1O_2$), which then goes on to oxidize CEES to CEESO.

Bulk-phase heterogeneous photocatalytic reactions (liquid suspensions of polymeric catalyst) were conducted using 0.8 weight % (2.5 mg) photocatalyst in 1 mL of CD_3OD under 1 bar oxygen with 0.2 mmol (23 μL) of CEES. All samples were irradiated with green (520−535 nm), royal blue (440−455 nm), or red (620−630 nm) LEDs with total powers of 450, 800, and 500 mW, respectively; reaction progress was monitored using ^{1}H and ^{13}C NMR spectroscopy (see the Supporting Information for details). Importantly, these reactions are selective for the desired nontoxic CEESO product (as well as ~1% of vinyl CEESO products); the toxic, doubly oxidized sulfone product ($CEESO_2$) was not observed by either ^{1}H or ^{13}C NMR spectroscopy. Table 2 summarizes the half-lives for CEES conversion using each BDP-PIM photocatalyst and red, green, or blue LEDs, and kinetic data are plotted in Figure 5.

https://doi.org/10.1021/acsami.1c21750
ACS Appl. Mater. Interfaces 2022, 14, 12596−12605

Table 2. Summary of the Photocatalytic Performances of the Polymers under Blue-, Green-, and Red-Light Irradiation

samples[a]	LED[b]	half-life (min)	irradiation time (min)	conv.[c] (%)
PIM-1	B	17	30	78
H-BDP-PIM	G/B	NA/28	30	24/54
Br-BDP-PIM	G/B	28/16	30	55/99
H-BDP-PIM-1a	G/B/R	NA/21/NA	30/30/40	30/73/10
Br-BDP-PIM-1a	R/G/B/B&G	66/15/8/6	95/30/15/12	80/99/99/99
H-BDP-PIM-1b	G/B	NA/26	30/30	6/59
Br-BDP-PIM-1b	G/B	23/5	30/10	71/99
Br-BDP-PIM-1b-F	G/B	20/4	45/12	95/98
H-BDP-PIM-1a-65C	G	NA	30	30

[a]F: Film. [b]B: Blue, G: green, and R: red. [c]Byproducts (≤1% conversion) such as vinyl compounds were disregarded in the conversion calculations.

Previously, we reported[17] that the halogenated BDP monomers exhibit excellent photocatalytic activity toward CEES oxidation with half-lives as short as 2 min under similar conditions. When synthesizing a polymer that contains two or more different photocatalytically active monomers, retaining the photocatalytic integrity of discrete monomers can be more challenging as a result of (i) aggregation-induced fluorescence quenching[48] and self-quenching,[49] (ii) charge-transfer-based fluorescence quenching,[50] (iii) increased opacity, which may limit the light absorption by active polymer units, (iv) differences in solubility, and (v) relatively slower transfer of reactive species to and from photocatalytic-active centers located in polymers. Also, potentially significant, but beyond the scope of our investigation are assessments of PIM particle size and methanol swelling on overall catalytic activity.[51] All the BDP-PIM derivatives possess permanent microporosity, while the optical studies reveal that the chromophores centered in the polymer backbones do not display the optical characteristics of aggregation. The BDP moieties remain powerful photocatalysts when incorporated into PIM backbones, particularly when PIMs bear halogenated BDP units, as a result of the more efficient ISC associated with the heavy Br atoms. Kinetics for the overall conversion from CEES to CEESO are slightly slower than those of the discrete molecular system. For example, Br-BDP-PIM converts 50% of CEES to CEESO in 28 min under green-light irradiation, while CEES conversion for H-BDP-PIM is just above 20% under analogous conditions (Figure 5d).

When **Br-BDP-PIM** is used as a photocatalyst under blue light, the half-life for CEES oxidation is cut nearly in half to 16 min (Figure 5d). This modest increase in performance is attributed to light absorption by TFTPN in the polymer backbone (Figure 2a), although the absence of the dicyanobenzene group within **Br-BDP-PIM** precludes the FRET-based mechanism that is present in the **H/Br-BDP-PIM-1a** and **-1b** analogues. In contrast, **Br-BDP-PIM-1a**,

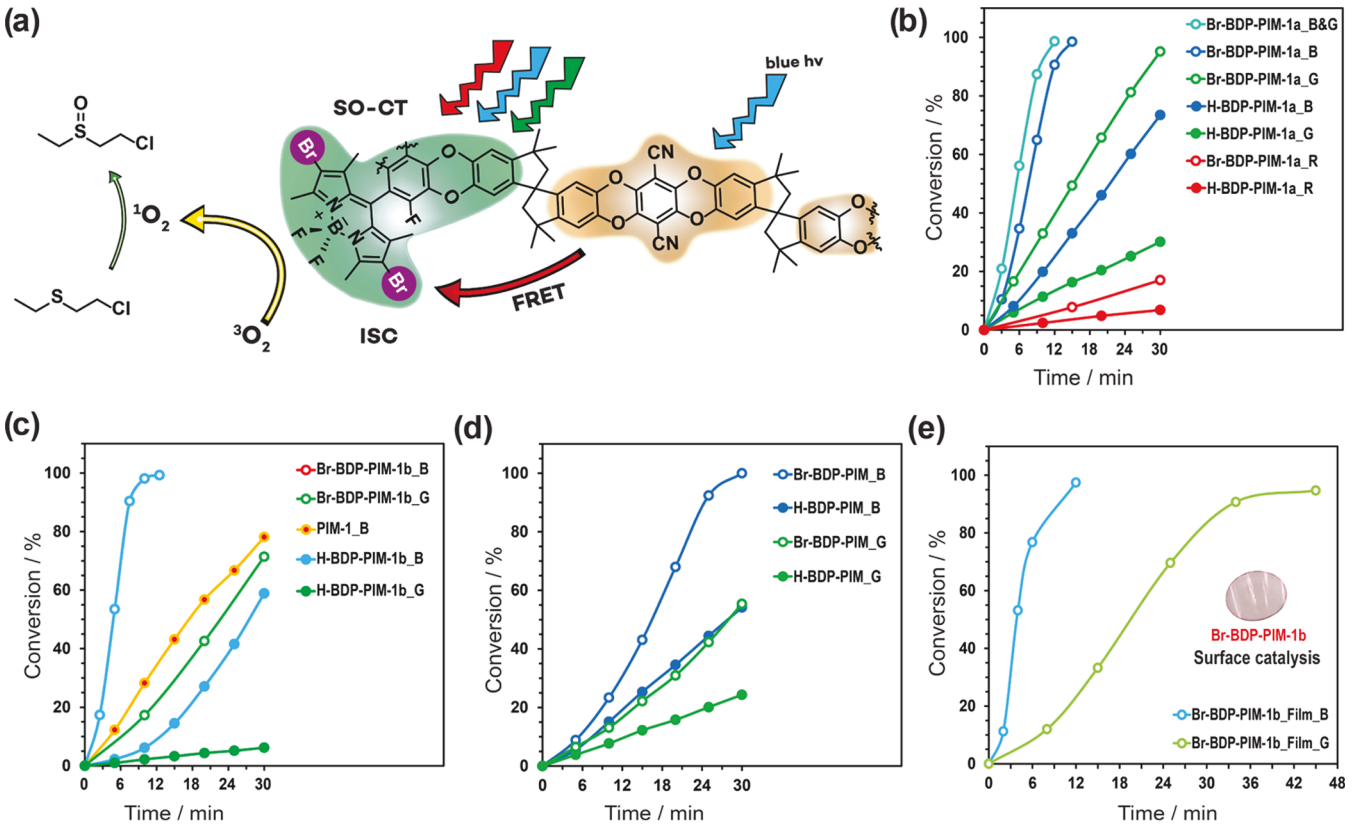

Figure 5. Representative scheme for the photocatalytic oxidation of the sulfur-mustard simulant CEES through energy transfer between the polymer backbone and the Br-BDP unit (a). The selective conversion of CEES to CEESO using **H-** and **Br-BDP-PIM-1b** and **PIM-1** (c) and **H-** and **Br-BDP-PIM** (d) polymers in the bulk form. The surface catalysis using **Br-BDP-PIM-1b** (e). Inset in (e) shows the PIM-coated glass layer (for higher resolution, see Figure S38). The catalysis conducted under blue and green-light irradiation is shown as B and G, respectively.

https://doi.org/10.1021/acsami.1c21750
ACS Appl. Mater. Interfaces 2022, 14, 12596−12605

which contains dicyanobenzene moieties in the polymer backbone, yields catalytic reaction half-lives of 15, 8, and 6 min for green, blue, and a combination of green and blue LEDs, respectively—a 2-fold improvement in photocatalytic performance compared to **Br-BDP-PIM** (Figure 5b). Faster reaction kinetics upon irradiation with a combination of green and blue LEDs may potentially result from improved CT and FRET from the polymer backbone to the BDP chromophore. In other words, simultaneous excitation of the polymer backbone and BDP absorption bands with blue and green light, respectively, leads to greater photon collection, greater population of the oxygen-sensitizing triplet excited state, and ultimately, an improvement in photocatalytic performance.

Irradiation of **Br-BDP-PIM-1b** with a green LED under these reaction conditions results in a half-life of 23 min for CEES conversion, which falls between the half-lives of 15 and 28 min observed for **Br-BDP-PIM-1a** and **Br-BDP-PIM**, respectively (Figure 5c). To probe the potential for undesired aggregation of pendant BDP units, we studied **Br-BDP-PIM-1b**, which contains fewer BDP units in the polymer compared to the amount present in **Br-BDP-PIM-1a**. Irradiation of **Br-BDP-PIM-1b** with the blue LED under analogous reaction conditions results in a half-life of 5 min, which is slightly shorter than the half-life of 8 min observed for **Br-BDP-PIM-1a**. In this case, the larger number of donor atoms in the polymer backbone results in more efficient FRET and better photocatalytic performance. These results are consistent with those in previous reports[33] in which increasing the donor/acceptor ratios in polymers leads to greater activity per chromophore, which is attributed to a combination of greater absorption by donor molecules and more efficient energy transfer from donor to acceptor units.

We also studied the photocatalytic activity of **PIM-1** to provide more context for the excellent performance observed for BDP-PIMs. Upon irradiation with the blue LED under analogous conditions, **PIM-1** exhibits a half-life for CEES oxidation of 17 min (Figure 5c). While this performance is subdued relative to that of BDP-based systems, this result demonstrates the excellent potential for the use of **PIM-1** as a polymeric building block in other photocatalytic systems. Moreover, this result highlights the synergistic effect between **PIM-1** and the BDP unit that enables the rapid detoxification of CEES.

Finally, we were interested in probing the performance of these materials as fully heterogeneous photocatalysts as this is a key consideration for developing detoxification catalysts to be used in practical settings (e.g., a reactive coating on a filter). We prepared **Br-BDP-PIM-1b** films on microscope lenses via spin-coating from chloroform solutions. CEES oxidation reactions were performed by placing a solution of 0.5 μL of CEES and 100 μL of CD_3OD on the film and then irradiating with green or blue light; the reaction products were collected with fresh CD_3OD for NMR analysis, with each film being used for a single data point. According to the kinetic data presented in Figure 5e, the half-life of CEES oxidation is about 20 min when irradiated with green light, and approximately 95% of the CEES is converted in 45 min. Similar to the solution-phase reactions, the desired CEESO comprises >98% of the product with the balance consisting of nontoxic vinyl derivatives of CEES and CEESO; none of the toxic sulfone product ($CEESO_2$) is observed. When the LED color is changed to blue, the half-life for CEES oxidation drops to 4 min, and nearly complete conversion is observed within 12 min. Overall, these results confirm that **Br-BDP-PIM-1b** films on surfaces can function as photocatalysts detoxification and transformation of CEES to CEESO.

CONCLUSIONS

Synthetically accessible under mild conditions is a new series of polymers of intrinsic microporosity that feature BDP chromophores and that are capable of functioning as heterogeneous photocatalysts. Heating DMF solutions of varying ratios of F5-BDP, TTSBI, and/or TFTPN comonomers over several days yields parent BDP-PIMs, which can then be brominated. The polymers exhibit permanent porosity, based on intentionally introduced tortuosity, rather than cross-linking, making them easy to solubilize, specifically in chloroform, and easy to recast as porous thin films. Both the pristine polymers and their brominated analogues display strong visible-region absorbance, together with ambient temperature fluorescence. Importantly, the emission spectra for both the pristine and brominated derivatives exhibit an emission peak at 760 nm that results from phosphorescence, indicating the ability to populate a triplet (T_1) excited state suitable for photosensitizing the formation of reactive singlet oxygen. Additionally, the incorporation of blue-light-harvesting dicyanobenzene units within the polymer engenders an efficient FRET to the BDP moieties. These excellent light absorption properties render this class of polymers effective as photocatalysts, both in solution and as thin films, for singlet-oxygen-based detoxification of the sulfur-mustard simulant CEES. In all cases, ^1H and ^{13}C NMR spectroscopic analysis of catalytic reaction mixtures confirms the selective oxidation of CEES to the nontoxic product CEESO with none of the toxic, doubly oxidized $CEESO_2$ observed. The excellent photocatalytic performance of BDP-based PIMs is attributable to a combination of (i) broad visible-region light absorption, (ii) efficient FRET from spirobisindane to BDP, (iii) longer wavelength light absorption by charge-transfer excitation, and (iv) SOC-enhanced (bromine-atom enhanced) intersystem crossing to form a triplet excited state capable of sensitizing the formation of reactive singlet oxygen. Overall, the study points to the ample potential for PIM-based chromophores, in solution suspended or thin-film form, for use as photocatalysts—potential that is underscored by the synthetic tunability of component monomers.

ASSOCIATED CONTENT

Supporting Information

The Supporting Information is available free of charge at https://pubs.acs.org/doi/10.1021/acsami.1c21750.

Materials/General Methods/Instrumentation, synthetic protocols and NMR spectroscopy, gas adsorption, thermogravimetric analysis (TGA), photophysical characterization, density functional theory (DFT) calculations, and photocatalytic studies (PDF)

AUTHOR INFORMATION

Corresponding Authors

Omar K. Farha − *Department of Chemistry, Northwestern University, Evanston, Illinois 60208-3113, United States;* orcid.org/0000-0002-9904-9845; Email: o-farha@northwestern.edu

Joseph T. Hupp − *Department of Chemistry, Northwestern University, Evanston, Illinois 60208-3113, United States;*

https://doi.org/10.1021/acsami.1c21750
ACS Appl. Mater. Interfaces 2022, 14, 12596−12605

orcid.org/0000-0003-3982-9812; Email: j-hupp@northwestern.edu

Authors

Ahmet Atilgan − *Department of Chemistry, Northwestern University, Evanston, Illinois 60208-3113, United States;* orcid.org/0000-0002-1531-3996

Yassine Beldjoudi − *Department of Chemistry, Northwestern University, Evanston, Illinois 60208-3113, United States;* orcid.org/0000-0002-9500-4308

Jierui Yu − *Department of Chemistry and Biochemistry, Southern Illinois University, Carbondale, Illinois 62901, United States*

Kent O. Kirlikovali − *Department of Chemistry, Northwestern University, Evanston, Illinois 60208-3113, United States;* orcid.org/0000-0001-8329-1015

Jacob A. Weber − *Department of Chemistry, Northwestern University, Evanston, Illinois 60208-3113, United States*

Jian Liu − *Department of Chemistry, Northwestern University, Evanston, Illinois 60208-3113, United States;* orcid.org/0000-0002-5024-1879

Dahee Jung − *Department of Chemistry, Northwestern University, Evanston, Illinois 60208-3113, United States;* orcid.org/0000-0003-1863-0193

Pravas Deria − *Department of Chemistry and Biochemistry, Southern Illinois University, Carbondale, Illinois 62901, United States;* orcid.org/0000-0001-7998-4492

Timur Islamoglu − *Department of Chemistry, Northwestern University, Evanston, Illinois 60208-3113, United States;* orcid.org/0000-0003-3688-9158

J. Fraser Stoddart − *Department of Chemistry, Northwestern University, Evanston, Illinois 60208-3113, United States; School of Chemistry, University of New South Wales, Sydney, NSW 2052, Australia;* orcid.org/0000-0003-3161-3697

Complete contact information is available at: https://pubs.acs.org/10.1021/acsami.1c21750

Notes

The authors declare no competing financial interest.

■ ACKNOWLEDGMENTS

The authors thank the personnel in the Integrated Molecular Structure Education and Research Center (IMSERC) at Northwestern University (NU) for their advice and assistance in data collection. O.K.F. and J.T.H. gratefully acknowledge support from the Defense Threat Reduction Agency under grant number [HDTRA1-19-1-0010]. J.F.S. thanks both KACST and NU for their support of this research. P.D. gratefully acknowledges funding from the National Science Foundation (NSF CAREER CHE-1944903).

■ REFERENCES

(1) Szinicz, L. History of Chemical and Biological Warfare Agents. *Toxicology* **2005**, *214*, 167−181.

(2) Masterson, J. Timeline of Syrian Chemical Weapons Activity, 2012-2020. https://www.armscontrol.org/factsheets/Timeline-of-Syrian-Chemical-Weapons-Activity (accessed Jan 25, 2021).

(3) Johnson, N. H.; Larsen, J. C.; Meek, E. Historical Perspective of Chemical Warfare Agents. In *Handbook of Toxicology of Chemical Warfare Agents*, 2nd ed.; Gupta, R. C., Ed.; Academic Press: Boston, 2015; Chapter 2, Vol. *285*, pp 7−15.

(4) Beldjoudi, Y.; Atilgan, A.; Weber, J. A.; Roy, I.; Young, R. M.; Yu, J.; Deria, P.; Enciso, A. E.; Wasielewski, M. R.; Hupp, J. T.; Stoddart, J. F. Supramolecular Porous Organic Nanocomposites for Heterogeneous Photocatalysis of a Sulfur Mustard Simulant. *Adv. Mater.* **2020**, *32*, No. 2001592.

(5) Thomas, A. Functional Materials: From Hard to Soft Porous Frameworks. *Angew. Chem., Int. Ed.* **2010**, *49*, 8328−8344.

(6) Chen, L.; Honsho, Y.; Seki, S.; Jiang, D. Light-Harvesting Conjugated Microporous Polymers: Rapid and Highly Efficient Flow of Light Energy with a Porous Polyphenylene Framework as Antenna. *J. Am. Chem. Soc.* **2010**, *132*, 6742−6748.

(7) Sakaushi, K.; Nickerl, G.; Wisser, F. M.; Nishio-Hamane, D.; Hosono, E.; Zhou, H.; Kaskel, S.; Eckert, J. An Energy Storage Principle using Bipolar Porous Polymeric Frameworks. *Angew. Chem., Int. Ed.* **2012**, *51*, 7850−7854.

(8) Rose, M. Nanoporous Polymers: Bridging the Gap between Molecular and Solid Catalysts? *ChemCatChem* **2014**, *6*, 1166−1182.

(9) Roeser, J.; Kailasam, K.; Thomas, A. Covalent Triazine Frameworks as Heterogeneous Catalysts for the Synthesis of Cyclic and Linear Carbonates from Carbon Dioxide and Epoxides. *ChemSusChem* **2012**, *5*, 1793−1799.

(10) Fischer, S.; Schmidt, J.; Strauch, P.; Thomas, A. An Anionic Microporous Polymer Network Prepared by the Polymerization of Weakly Coordinating Anions. *Angew. Chem., Int. Ed.* **2013**, *52*, 12174−12178.

(11) Kundu, D. S.; Schmidt, J.; Bleschke, C.; Thomas, A.; Blechert, S. A Microporous Binol-Derived Phosphoric Acid. *Angew. Chem., Int. Ed.* **2012**, *51*, 5456−5459.

(12) Fischer, S.; Schimanowitz, A.; Dawson, R.; Senkovska, I.; Kaskel, S.; Thomas, A. Cationic Microporous Polymer Networks by Polymerisation of Weakly Coordinating Cations with CO2-storage Ability. *J. Mater. Chem. A* **2014**, *2*, 11825−11829.

(13) Rabbani, M. G.; Sekizkardes, A. K.; Kahveci, Z.; Reich, T. E.; Ding, R.; El-Kaderi, H. M. A 2D Mesoporous Imine-Linked Covalent Organic Framework for High Pressure Gas Storage Applications. *Chem. - Eur. J.* **2013**, *19*, 3324−3328.

(14) Garibay, S. J.; Weston, M. H.; Mondloch, J. E.; Colón, Y. J.; Farha, O. K.; Hupp, J. T.; Nguyen, S. T. Accessing Functionalized Porous Aromatic Frameworks (PAFs) through a de novo approach. *CrystEngComm* **2013**, *15*, 1515−1519.

(15) Lu, W.; Sculley, J. P.; Yuan, D.; Krishna, R.; Wei, Z.; Zhou, H.-C. Polyamine-Tethered Porous Polymer Networks for Carbon Dioxide Capture from Flue Gas. *Angew. Chem., Int. Ed.* **2012**, *51*, 7480−7484.

(16) Chen, Q.; Luo, M.; Hammershøj, P.; Zhou, D.; Han, Y.; Laursen, B. W.; Yan, C.-G.; Han, B.-H. Microporous Polycarbazole with High Specific Surface Area for Gas Storage and Separation. *J. Am. Chem. Soc.* **2012**, *134*, 6084−6087.

(17) Atilgan, A.; Cetin, M. M.; Yu, J.; Beldjoudi, Y.; Liu, J.; Stern, C. L.; Cetin, F. M.; Islamoglu, T.; Farha, O. K.; Deria, P.; Stoddart, J. F.; Hupp, J. T. Post-Synthetically Elaborated BODIPY-Based Porous Organic Polymers (POPs) for the Photochemical Detoxification of a Sulfur Mustard Simulant. *J. Am. Chem. Soc.* **2020**, *142*, 18554−18564.

(18) Yang, Y.; Zhang, Q.; Zheng, J.; Zhang, S. Synthesis and Characterization of Pyrrole-Containing Microporous Polymeric Networks. *Polymer* **2013**, *54*, 3254−3260.

(19) Gu, C.; Chen, Y.; Zhang, Z.; Xue, S.; Sun, S.; Zhang, K.; Zhong, C.; Zhang, H.; Pan, Y.; Lv, Y.; Yang, Y.; Li, F.; Zhang, S.; Huang, F.; Ma, Y. Electrochemical Route to Fabricate Film-Like Conjugated Microporous Polymers and Application for Organic Electronics. *Adv. Mater.* **2013**, *25*, 3443−3448.

(20) Becker, D.; Heidary, N.; Horch, M.; Gernert, U.; Zebger, I.; Schmidt, J.; Fischer, A.; Thomas, A. Microporous Polymer Network Films Covalently Bound to Gold Electrodes. *Chem. Commun.* **2015**, *51*, 4283−4286.

(21) Budd, P. M.; Ghanem, B. S.; Makhseed, S.; McKeown, N. B.; Msayib, K. J.; Tattershall, C. E. Polymers of Intrinsic Microporosity (PIMs): Robust, Solution-processable, Organic Nanoporous Materials. *Chem. Commun.* **2004**, 230−231.

(22) Budd, P. M.; McKeown, N. B.; Fritsch, D. Free Volume and Intrinsic Microporosity In Polymers. *J. Mater. Chem.* **2005**, *15*, 1977−1986.

(23) Weber, J.; Schmidt, J.; Thomas, A.; Böhlmann, W. Micropore Analysis of Polymer Networks by Gas Sorption and ^{129}Xe NMR Spectroscopy: Toward a Better Understanding of Intrinsic Microporosity. *Langmuir* **2010**, *26*, 15650−15656.
(24) Smith, J. D.; Jamhawi, A. M.; Jasinski, J. B.; Gallou, F.; Ge, J.; Advincula, R.; Liu, J.; Handa, S. Organopolymer with Dual Chromophores and Fast Charge-transfer Properties for Sustainable Photocatalysis. *Nat. Commun.* **2019**, *10*, No. 1837.
(25) Song, Q.; Cao, S.; Zavala-Rivera, P.; Ping Lu, L.; Li, W.; Ji, Y.; Al-Muhtaseb, S. A.; Cheetham, A. K.; Sivaniah, E. Photo-oxidative Enhancement of Polymeric Molecular Sieve Membranes. *Nat. Commun.* **2013**, *4*, No. 1918.
(26) Kamkaew, A.; Lim, S. H.; Lee, H. B.; Kiew, L. V.; Chung, L. Y.; Burgess, K. BODIPY Dyes in Photodynamic Therapy. *Chem. Soc. Rev.* **2013**, *42*, 77−88.
(27) Loudet, A.; Burgess, K. BODIPY Dyes and Their Derivatives: Synthesis and Spectroscopic Properties. *Chem. Rev.* **2007**, *107*, 4891−4932.
(28) Atilgan, A.; Eçik, E. T.; Guliyev, R.; Uyar, T. B.; Erbas-Cakmak, S.; Akkaya, E. U. Near-IR-Triggered, Remote-Controlled Release of Metal Ions: A Novel Strategy for Caged Ions. *Angew. Chem., Int. Ed.* **2014**, *53*, 10678−10681.
(29) Wang, H.; Wagner, G. W.; Lu, A. X.; Nguyen, D. L.; Buchanan, J. H.; McNutt, P. M.; Karwacki, C. J. Photocatalytic Oxidation of Sulfur Mustard and Its Simulant on BODIPY-Incorporated Polymer Coatings and Fabrics. *ACS Appl. Mater. Interfaces* **2018**, *10*, 18771−18777.
(30) Atilgan, A.; Islamoglu, T.; Howarth, A. J.; Hupp, J. T.; Farha, O. K. Detoxification of a Sulfur Mustard Simulant Using a BODIPY-Functionalized Zirconium-Based Metal−Organic Framework. *ACS Appl. Mater. Interfaces* **2017**, *9*, 24555−24560.
(31) Li, W.; Li, L.; Xiao, H.; Qi, R.; Huang, Y.; Xie, Z.; Jing, X.; Zhang, H. Iodo-BODIPY: A Visible-light-driven, Highly Efficient and Photostable Metal-free Organic Photocatalyst. *RSC Adv.* **2013**, *3*, 13417−13421.
(32) Filatov, M. A.; Karuthedath, S.; Polestshuk, P. M.; Savoie, H.; Flanagan, K. J.; Sy, C.; Sitte, E.; Telitchko, M.; Laquai, F.; Boyle, R. W.; Senge, M. O. Generation of Triplet Excited States via Photoinduced Electron Transfer in meso-anthra-BODIPY: Fluorogenic Response toward Singlet Oxygen in Solution and in Vitro. *J. Am. Chem. Soc.* **2017**, *139*, 6282−6285.
(33) Lifschitz, A. M.; Young, R. M.; Mendez-Arroyo, J.; Roznyatovskiy, V. V.; McGuirk, C. M.; Wasielewski, M. R.; Mirkin, C. A. Chemically Regulating Rh(I)-BODIPY Photoredox Switches. *Chem. Commun.* **2014**, *50*, 6850−6852.
(34) Chen, K.; Yang, W.; Wang, Z.; Iagatti, A.; Bussotti, L.; Foggi, P.; Ji, W.; Zhao, J.; Donato, M. D. Triplet Excited State of BODIPY Accessed by Charge Recombination and Its Application in Triplet−Triplet Annihilation Upconversion. *J. Phys. Chem. A* **2017**, *121*, 7550−7564.
(35) Thivierge, C.; Loudet, A.; Burgess, K. Brilliant BODIPY−Fluorene Copolymers with Dispersed Absorption and Emission Maxima. *Macromolecules* **2011**, *44*, 4012−4015.
(36) Cui, X.; Zhang, C.; Xu, K.; Zhao, J. Application of Singlet Energy Transfer in Triplet State Formation: Broadband Visible Light-Absorbing Triplet photosensitizers, Molecular Structure Design, Related Photophysics and Applications. *J. Mater. Chem. C* **2015**, *3*, 8735−8759.
(37) Budd, P. M.; Elabas, E. S.; Ghanem, B. S.; Makhseed, S.; McKeown, N. B.; Msayib, K. J.; Tattershall, C. E.; Wang, D. Solution-Processed, Organophilic Membrane Derived from a Polymer of Intrinsic Microporosity. *Adv. Mater.* **2004**, *16*, 456−459.
(38) El-Ali, H. A. A.; Jing, J.; Zhang, X. Solid-state Emissive O-BODIPY Dyes with Bimodal Emissions Across Red and Near Infrared Region. *RSC Adv.* **2019**, *9*, 16246−16251.
(39) To better understand the role of the temperature in this reaction, the polymerization reaction for **H-BDP-PIM-1a** (monomer ratio of F5-BDP:TFTPN:TTSBI = 1:2:3) was initially performed at 65°C for 2 days to yield **H-BDP-PIM-1a-65C**, which is soluble in THF but insoluble in chloroform and methanol. When the reaction time is extended to 4 days at 65°C, the resulting polymers exhibit low solubility in THF, and this decrease in solubility time suggests potential cross-linkages among the polymer chains that form with longer reaction times under these conditions. As a result, the temperature was lowered to 50-55°C in order to minimize the formation of undesired cross-linkages in the polymers (see the Supporting Information for more details regarding reaction procedures and solubility properties of the polymers).
(40) In other words, the nucleophilic spirobisindane monomers are capable of an S_N2 substitution on the boron atom of the BODIPY core within both **H-BDP-PIM** and **H-BDP-PIM-1a** under these reaction conditions. The relative integrations of these two peaks in the ^{11}B NMR spectrum of **H-BDP-PIM-1a** suggest present BODIPY moiety in the polymer partially undergoes spirobisindane substitution (Figure S7).
(41) Du, N.; Robertson, G. P.; Pinnau, I.; Guiver, M. D. Polymers of Intrinsic Microporosity Derived from Novel Disulfone-Based Monomers. *Macromolecules* **2009**, *42*, 6023−6030.
(42) Zhang, P.; Jiang, X.; Wan, S.; Dai, S. Charged Porous Polymers using a Solid C−O Cross-Coupling Reaction. *Chem. - Eur. J.* **2015**, *21*, 12866−12870.
(43) Du, N.; Robertson, G. P.; Song, J.; Pinnau, I.; Thomas, S.; Guiver, M. D. Polymers of Intrinsic Microporosity Containing Trifluoromethyl and Phenylsulfone Groups as Materials for Membrane Gas Separation. *Macromolecules* **2008**, *41*, 9656−9662.
(44) Thommes, M.; Kaneko, K.; Neimark, A. V.; Olivier, J. P.; Rodriguez-Reinoso, F.; Rouquerol, J.; Sing, K. S. W. Physisorption of Gases, with Special Reference to the Evaluation of Surface Area and Pore Size Distribution (IUPAC Technical Report). *Pure Appl. Chem.* **2015**, *87*, 1051−1069.
(45) Hou, Y.; Kurganskii, I.; Elmali, A.; Zhang, H.; Gao, Y.; Lv, L.; Zhao, J.; Karatay, A.; Luo, L.; Fedin, M. Electronic Coupling and Spin−orbit Charge Transfer Intersystem Crossing (SOCT-ISC) in Compact BDP−carbazole Dyads with Different Mutual Orientations of the Electron Donor and Acceptor. *J. Chem. Phys.* **2020**, *152*, No. 114701.
(46) Baroncini, M.; Bergaminia, G.; Ceroni, P. Rigidification or Interaction-induced Phosphorescence of Organic Molecules. *Chem. Commun.* **2017**, *53*, 2081−2093.
(47) Austin, A.; Petersson, G. A.; Frisch, M. J.; Dobek, F. J.; Scalmani, G.; Throssell, K. A Density Functional with Spherical Atom Dispersion Terms. *J. Chem. Theory Comput.* **2012**, *8*, 4989−5007.
(48) Nie, H.; Hu, K.; Cai, Y.; Peng, Q.; Zhao, Z.; Hu, R.; Chen, J.; Su, S.-J.; Qin, A.; Tang, B. Z. Tetraphenylfuran: Aggregation-Induced Emission or Aggregation-Caused Quenching? *Mater. Chem. Front.* **2017**, *1*, 1125−1129.
(49) Zhuang, X.; Ha, T.; Kim, H. D.; Centner, T.; Labeit, S.; Chu, S. Fluorescence Quenching: A Tool for Single-molecule Protein-folding Study. *Proc. Natl. Acad. Sci. U.S.A.* **2000**, *97*, 14241−14244.
(50) Santra, D. C.; Bera, M. K.; Sukul, P. K.; Malik, S. Charge-Transfer-Induced Fluorescence Quenching of Anthracene Derivatives and Selective Detection of Picric Acid. *Chem. - Eur. J.* **2016**, *22*, 2012−2019.
(51) Woods, D. J.; Hillman, S. A. J.; Pearce, D.; Flagg, L. Q.; Duffy, W.; McCulloch, I.; Durrant, J. R.; Guilbert, A. A. Y.; Zwijnenburg, M. A.; Sprick, R. S.; Nelson, J.; Cooper, A. I.; Wilbraham, L. Side-chain Tuning in Conjugated Polymer Photocatalysts for Improved Hydrogen Production from Water. *Energy Environ. Sci.* **2020**, *13*, 1843−1855.

https://doi.org/10.1021/acsami.1c21750
ACS Appl. Mater. Interfaces 2022, 14, 12596−12605